"Belt and Braces": A Peptide-Based Linker System of de Novo Design

ARTICLE *in* JOURNAL OF THE AMERICAN CHEMICAL SOCIETY · SEPTEMBER 2003

Impact Factor: 12.11 · DOI: 10.1021/ja0352045 · Source: PubMed

4 AUTHORS, INCLUDING:

Maxim G Ryadnov
National Physical Laboratory
74 PUBLICATIONS **1,292** CITATIONS

SEE PROFILE

J|A|C|S
ARTICLES
Published on Web 07/09/2003

"Belt and Braces": A Peptide-Based Linker System of de Novo Design

Maxim G. Ryadnov,[†] Buelent Ceyhan,[‡] Christof M. Niemeyer,*[,‡] and Derek N. Woolfson*[,†]

Contribution from the Center for Biomolecular Design and Drug Development, School of Biological Sciences, University of Sussex, Falmer BN1 9QG, United Kingdom, and Universität Dortmund, FB Chemie, Biologisch-Chemische Mikrostrukturtechnik, Otto-Hahn-Strasse 6, D-44227 Dortmund, Germany

Received March 18, 2003; E-mail: dek@biols.sussex.ac.uk; cmn@chemie.uni-dortmund.de

Abstract: A new self-assembling peptide-based linker is described. The system comprises three leucine-zipper sequences of de novo design: one peptide, "the belt", templates the co-assembly of the other two-half-sized peptides, "the braces". These basic features were confirmed by circular dichroism spectroscopy and analytical ultracentrifugation: when mixed, the three peptides reversibly formed a predominantly helical and stable 1:1:1 ternary complex. Surface plasmon resonance experiments demonstrated assembly of the complex on gold surfaces, while the ability of the system to bring together peptide-bound cargo was demonstrated using colloidal gold nanoparticles. In the latter experiments, the nanoparticles were derivatized with the brace peptides prior to the addition of the belt. Transmission electron microscopy images of the resulting networks revealed regular ~7 nm separations between adjacent particles, consistent with the 42-amino acid helical design of the belt and braces. To our knowledge, belt and braces is a novel concept in leucine-zipper assembly and the first example of employing peptides to guide nanoparticle assembly.

Introduction

Biomolecular recognition systems, such as nucleic-acid hybridization and protein−ligand interactions, are being utilized in biosensor[1] and microarray technology.[2−7] There is also interest in using biomolecules as components in supramolecular self-assembly to generate novel components for the development of advanced functional materials and molecular electronics.[8,9] A key driver in these fields is the demand for smaller, cheaper, and more complex components. It is widely accepted that such improvements will not be fully realized using conventional "top-down" methods (e.g., photolithography), but will require fundamentally new approaches for the fabrication of electronic and other components. Consequently, complementary "bottom-up" technologies are being explored as potential ways for fabricating nanometer-sized devices.[10,11] These are based on the self-assembly of small molecular building blocks to form larger functional elements. Biomolecules have been established as effective tools for mediating supramolecular assembly of molecular and colloidal components.[8] In particular, due to the specificity of Watson−Crick base-pairing, DNA oligonucleotides have unique and predictable self-recognition capabilities that make them promising starting materials for constructing well-defined nanostructures[12] and assemblies of metal and semiconductor nanoparticles.[8,13,14]

One concept for using biomolecules to assemble nanoparticles is illustrated in Figure 1a: nanoparticles are functionalized with individual recognition groups that are complementary for a separate molecular linker. Addition of the linker drives assembly of the particles to form extended networks, which, in some cases, grow to macroscopic materials. Mirkin's group has pioneered this approach using oligonucleotide-based recognition motifs and has successfully applied it to the solution-phase assembly of nanoparticles[15−21] and the directed immobilization of nano-

[†] University of Sussex.
[‡] Universität Dortmund.

(1) *Frontiers in Biosensors: Fundamental Aspects*; Scheller, F. W., Schaubert, F., Fredrowitz, J., Eds.; Birkhäuser Verlag: Boston, 1997.
(2) Holloway, A. J.; Van Laar, R. K.; Tothill, R. W.; Bowtell, D. D. *Nat. Genet.* **2002**, *32 Suppl 2*, 481−489.
(3) Pirrung, M. C. *Angew. Chem., Int. Ed.* **2002**, *41*, 1276−1289.
(4) Mirzabekov, A.; Kolchinsky, A. *Curr. Opin. Chem. Biol.* **2002**, *6*, 70−75.
(5) Templin, M. F.; Stoll, D.; Schrenk, M.; Traub, P. C.; Vohringer, C. F.; Joos, T. O. *Trends Biotechnol.* **2002**, *20*, 160−166.
(6) Lam, K. S.; Renil, M. *Curr. Opin. Chem. Biol.* **2002**, *6*, 353−358.
(7) Winssinger, N.; Ficarro, S.; Schultz, P. G.; Harris, J. L. *Proc. Natl. Acad. Sci. U.S.A.* **2002**, *99*, 11139−11144.
(8) Niemeyer, C. M. *Angew. Chem., Int. Ed.* **2001**, *40*, 4128−4158.
(9) Niemeyer, C. M. *Science* **2002**, *297*, 62−63.
(10) Moore, G. E. *Electronics* **1965**, *38*, 114−116.
(11) Whitesides, G. M.; Mathias, J. P.; Seto, C. T. *Science* **1991**, *254*, 1312−1319.
(12) Seeman, N. C. *Nano Lett.* **2001**, *1*, 22−26.
(13) Mirkin, C. A. *Inorg. Chem.* **2000**, *39*, 2258−2272.
(14) Gerion, D.; Parak, W. J.; Williamson, S. C.; Zanchet, D.; Micheel, C. M.; Alivisatos, A. P. *J. Am. Chem. Soc.* **2002**, *124*, 7070−7074.
(15) Mirkin, C. A.; Letsinger, R. L.; Mucic, R. C.; Storhoff, J. J. *Nature* **1996**, *382*, 607−609.
(16) Elghanian, R.; Storhoff, J. J.; Mucic, R. C.; Letsinger, R. L.; Mirkin, C. A. *Science* **1997**, *277*, 1078−1081.
(17) Mucic, R. C.; Storhoff, J. J.; Mirkin, C. A.; Letsinger, R. L. *J. Am. Chem. Soc.* **1998**, *120*, 12674−12675.
(18) Storhoff, J. J.; Elghanian, R.; Mucic, R. C.; Mirkin, C. A.; Letsinger, R. L. *J. Am. Chem. Soc.* **1998**, *120*, 1959−1964.
(19) Mitchell, G. P.; Mirkin, C. A.; Letsinger, R. L. *J. Am. Chem. Soc.* **1999**, *121*, 8122−8123.
(20) Reynolds, R. A.; Mirkin, C. A.; Letsinger, R. L. *J. Am. Chem. Soc.* **2000**, *122*, 3795−3796.
(21) Storhoff, J. J.; Lazarides, A. A.; Mucic, R. C.; Mirkin, C. A.; Letsinger, R. L.; Schatz, G. C. *J. Am. Chem. Soc.* **2000**, *122*, 4640−4650.

10.1021/ja0352045 CCC: $25.00

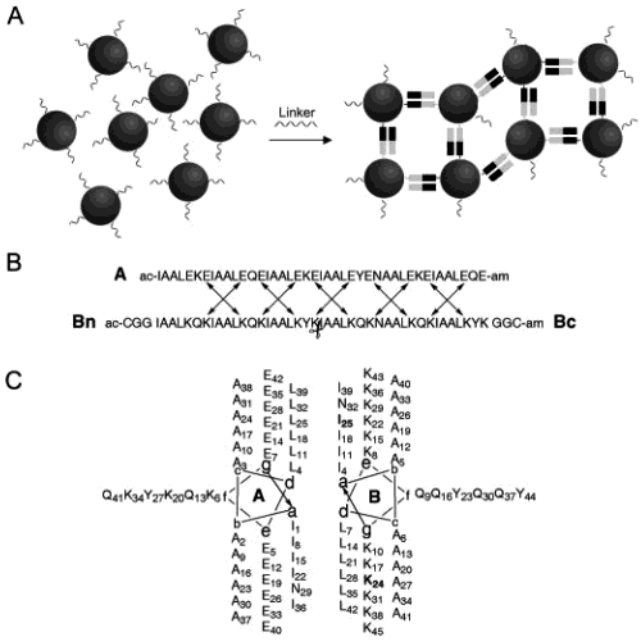

Figure 1. Linker-mediated assembly of nanoparticles. (A) A concept for assembling nanoparticles using biomolecular linkers (see text). (B and C) The belt-and-braces peptide design. (B) The linear sequences of the belt (**A**) and brace ($\mathbf{B_N}$ and $\mathbf{B_C}$) peptides. Designed interpeptide electrostatic interactions are depicted by double-headed arrows. The break between the $\mathbf{B_N}$ and $\mathbf{B_C}$ peptides is indicated by scissors. In (C), the sequences are drawn out on a 3.5-residue-per-turn helical wheel to show how the interfacial *a*, *d*, *e*, and *g* positions of the heptad repeats come together. The break between the $\mathbf{B_N}$ and $\mathbf{B_C}$ peptides occurs between K_{24} and I_{25}, which are highlighted bold.

particles on solid substrates, which allows for the fast and sensitive detection of nucleic acid analytes.[22−25]

As the relationships between the primary and three-dimensional structures of peptides and proteins are less clear than those for DNA, it is not straightforward to envisage how polypeptides might be employed in the above scheme. Nonetheless, some similar strategies have been explored using protein-based recognition systems, in particular, antibody−antigen[26] and streptavidin−biotin interactions.[27−29] Directed molecular evolution strategies have also been applied to develop peptides that recognize the inorganic surfaces of semiconductors[30,31] and metal[32] nanoparticles, thus allowing the mediated growth of hybrid supramolecular networks. However, these approaches have drawbacks, and none provides a general means to achieve efficient biomimetic assembly of molecular and colloidal components. Exploring novel linker systems would enrich the kit of methodologies leading to the determination of easily reproducible principles for biomolecular-directed assembly. In addition, peptide-based linking systems introduce the possibility of recombinant protein production and, with it, the possibility of producing functional protein fusions as building blocks for new bioinspired materials.

Here, we report the rational design of a peptide recognition system based on a three-component coiled-coil assembly, which we refer to as "belt and braces" (Figure 1). In terms of peptide and protein structure, coiled-coil assemblies are relatively simple, and sequence-to-structure relationships are available that permit their prediction and design. Briefly, coiled coils are bundles of between two and five amphipathic helices, which assemble through their hydrophobic faces, Figure 1C.[33,34] The nature of the residues at the interface determines the coiled-coil oligomer state, helix orientation, and partner selection.[33−40] The simplest and best understood coiled coils are the two-stranded, parallel leucine zippers. On the basis of our understanding of leucine zippers, we designed a "belt" peptide to template the bringing together of two "brace" peptides. We demonstrate specific assembly of the ternary complex as well as its utility in peptide-directed immobilization at surfaces and the assembly of nanoparticles.

Results

Peptide Design. Our aim was to engineer a peptide-based linker system of three components: one fragment, the belt (**A**, Figure 1B), would act as the template for the assembly of two half-sized fragments, the braces ($\mathbf{B_N}$ and $\mathbf{B_C}$). Others have introduced a similar approach to make self-replicating peptides.[41] Coiled coils, specifically leucine-zipper motifs, are ideal candidates for such designs because principles are available that link coiled-coil sequence and structure.[33−40] We built on our own experience in leucine-zipper design[42−45] to engineer the belt-and-braces system. This process involved engineering both toward the desired structure (positive design) and away from alternate structures (negative design);[42,46] for instance, the possibilities for autonomous folding of the individual peptide components, or nonproductive co-assembly of pairs of components, had to be minimized. The resulting design had the following features, Figure 1B and C: first, the sequences contained heptad repeats, *abcdefg*, typical of canonical coiled coils. In this notation, residues at *a* and *d* and at *e* and *g* contribute to the helix−helix interface, Figure 1C, and are usually hydrophobic and charged, respectively. Four or more contiguous repeats usually produce stable assemblies.[47] We

(22) Taton, T. A.; Mucic, R. C.; Mirkin, C. A.; Letsinger, R. L. *J. Am. Chem. Soc.* **2000**, *122*, 6305−6306.
(23) Taton, T. A.; Mirkin, C. A.; Letsinger, R. L. *Science* **2000**, *289*, 1757−1760.
(24) Taton, T. A.; Lu, G.; Mirkin, C. A. *J. Am. Chem. Soc.* **2001**, *123*, 5164−5165.
(25) Park, S. J.; Taton, T. A.; Mirkin, C. A. *Science* **2002**, *295*, 1503−1506.
(26) Shenton, W.; Davies, S. A.; Mann, S. *Adv. Mater.* **1999**, *11*, 449−452.
(27) Niemeyer, C. M.; Bürger, W.; Peplies, J. *Angew. Chem., Int. Ed.* **1998**, *37*, 2265−2268.
(28) Connolly, S.; Fitzmaurice, D. *Adv. Mater.* **1999**, *11*, 1202−1205.
(29) Niemeyer, C. M.; Ceyhan, B. *Angew. Chem., Int. Ed.* **2001**, *40*, 3685−3688.
(30) Lee, S. W.; Mao, C.; Flynn, C. E.; Belcher, A. M. *Science* **2002**, *296*, 892−895.
(31) Whaley, S. R.; English, D. S.; Hu, E. L.; Barbara, P. F.; Belcher, A. M. *Nature* **2000**, *405*, 665−666.
(32) Brown, S. *Nano Lett.* **2001**, *1*, 391−394.
(33) Lupas, A. *Trends Biochem. Sci.* **1996**, *21*, 375−382.
(34) Walshaw, J.; Woolfson, D. N. *Protein Sci.* **2001**, *10*, 668−673.
(35) O'Shea, E. K.; Lumb, K. J.; Kim, P. S. *Curr. Biol.* **1993**, *3*, 658−667.
(36) Harbury, P. B.; Zhang, T.; Kim, P. S.; Alber, T. *Science* **1993**, *262*, 1401−1407.
(37) Woolfson, D. N.; Alber, T. *Protein Sci.* **1995**, *4*, 1596−1607.
(38) Kim, B. M.; Oakley, M. G. *J. Am. Chem. Soc.* **2002**, *124*, 8237−8244.
(39) Monera, O. D.; Kay, C. M.; Hodges, R. S. *Biochemistry* **1994**, *33*, 3, 3862−3871.
(40) Gonzalez, L.; Woolfson, D. N.; Alber, T. *Nat. Struct. Biol.* **1996**, *3*, 1011−1018.
(41) Saghatelian, A.; Yokobayashi, Y.; Soltani, K.; Ghadiri, M. R. *Nature* **2001**, *409*, 797−801.
(42) Nautiyal, S.; Woolfson, D. N.; King, D. S.; Alber, T. *Biochemistry* **1995**, *34*, 11645−11651.
(43) Pandya, M. J.; Spooner, G. M.; Sunde, M.; Thorpe, J. R.; Roger, A.; Woolfson, D. N. *Biochemistry* **2000**, *39*, 8728−8734.
(44) Ciani, B.; Hutchinson, E. G.; Sessions, R. B.; Woolfson, D. N. *J. Biol. Chem.* **2002**, *277*, 10150−10155.
(45) Hicks, M. R.; Holberton, D. V.; Kowalczyk, C.; Woolfson, D. N. *Fold Des.* **1997**, *2*, 149−158.
(46) Beasley, J. R.; Hecht, M. H. *J. Biol. Chem.* **1997**, *272*, 2031−2034.
(47) Litowski, J. R.; Hodges, R. S. *J. Pept. Res.* **2001**, *58*, 477−492.

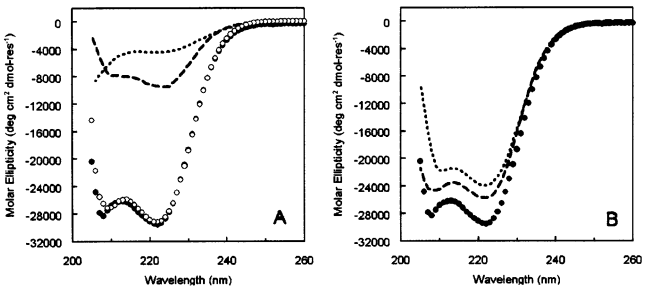

Figure 2. Peptide assembly probed by CD spectroscopy. (A) Spectra for the individual belt peptide (broken line), a 1:1 mixture of the braces (dotted line), and the 1:1:1 mixture of all three peptides (●). The ○ symbols show the spectrum of the latter after thermal unfolding and cooling. (B) Spectra for one of the two-component mixtures, $\mathbf{B_N}$ plus the belt in 1:1 (dotted line) and 2:1 (dashed line) ratios; ● are as in (A). Samples were 100 μM in each peptide, 10 mM MOPS, 1 mM DTT, pH 7, and at 5 °C.

settled on a six-heptad design for the belt and braces: the belt comprised six heptads, while the braces had three each. Second, to direct a parallel, two-helix (leucine-zipper) structure, all but one of the *a* sites was made isoleucine and all of the *d* were made leucine.[36,37] Third, to prevent autonomous folding and to encourage ternary assembly, the *e* and *g* positions of the belt were all made negatively charged (glutamic acid), while the corresponding sites of the braces were all made basic (lysine). Fourth, to distinguish the interactions of the two braces and the belt, the central *a* site of the C-terminal brace ($\mathbf{B_C}$) was made asparagine, as was its complement, the fifth *a* position in the belt; although destabilizing, the resulting asparagine−asparagine interaction is highly specifying.[40,43,48,49] Fifth, the remaining *b*, *c*, and *f* positions were made combinations of alanine, glutamic acid, and lysine; one *f* site in each peptide was reserved for a tyrosine chromophore. Sixth, to allow derivatization, CysGlyGly and GlyGlyCys tags were added to the N- and C-termini of $\mathbf{B_N}$ and $\mathbf{B_C}$, respectively. Finally, except for the C- and N-termini of $\mathbf{B_N}$ and $\mathbf{B_C}$, respectively, the termini of all of the peptides were capped.

Solution-Phase Assembly of Belt and Braces. Circular dichroism (CD) spectroscopy provides a convenient probe of α-helical structure in leucine-zipper systems.[50] Consistent with the design concept, none of the individual belt-and-braces peptides nor the combination of the two braces showed appreciable α-helix in solution by CD spectroscopy, Figure 2A. However, equimolar mixtures of all three peptides gave CD spectra indicative of considerable α-helix formation, Figure 2A. Furthermore, as was expected for an oligomerizing system, the amount of helix was concentration dependent: based on the CD signal at 222 nm ($[\theta]_{222}$),[51] the percent helix for samples 20, 100, and 200 μM in each peptide were ∼70%, ∼80%, and ∼85%, respectively; these values were consistent with TFE-induced helix formation, which gave a benchmark for the upper limit of the $[\theta]_{222}$ in our system of ∼−32 000 deg cm^2 dmol^{-1}.[45,52]

Thermal denaturation of leucine-zipper peptides as followed by the loss of $[\theta]_{222}$ with increasing temperature provides a measure of stability and cooperativity of assembly. The thermal unfolding of 1:1:1 mixtures of the belt-and-braces peptides gave sigmoidal unfolding curves as was expected for a unique, cooperatively folded structure, Figure 3. Importantly, low-temperature CD spectra recorded before and after thermal unfolding were very similar, Figure 2A, indicating almost complete reversibility of unfolding. The first derivatives of the unfolding curves were dominated by a single peak revealing transition midpoints (T_M) of 60 ± 2 °C, Figure 3. Unexpectedly, however, the T_M was similar at 20 and 100 μM peptide, and the peaks had some structure possibly suggestive of partial unfolding or fraying of the helical assemblies. However, this behavior was much more marked for the binary mixtures, for example, $\mathbf{A} + \mathbf{B_N}$ (Figure 1S, Supporting Information). These gave approximately linear thermal denaturation curves, which probably comprised several overlapping transitions and were consistent with the formation of two or more nonspecific complexes.

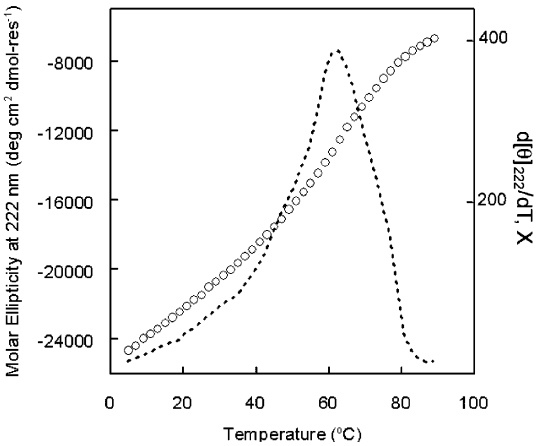

Figure 3. Thermal unfolding of the 20 μM belt-and-braces complex. ○ symbols show the raw CD data, and the broken line gives the first derivative.

The oligomerization states of the belt-and-braces peptides were probed by sedimentation equilibrium analysis in an analytical ultracentrifuge. In these experiments, all samples were 100 μM in each peptide, 10 mM MOPS, 1 mM DTT, pH 7, and at 5 °C. Sedimentation equilibrium data were fitted assuming a single ideal species. The returned molecular weights for the belt alone and for the 1:1 mixture of the braces were consistent with the design and the foregoing CD data; that is, all peptides behaved as monomers and fitted the models well; the experimental molecular weights were 4875 Da (95% confidence limits 4592 and 5157) for the belt, and 2690 Da (2518 and 2857) for the braces, respectively, as compared to the calculated relative molecular masses of 4624 for the belt, and 2570 and 2528 for the braces. The molecular weight returned for the 1:1:1 mixture, 9204 Da (9020 and 9387), was close to that expected for the 1:1:1 ternary complex (9722 Da). However, the residual signal (experimental data minus the fitted curve) showed a systematic error typical of an associating system (Figure 2S, Supporting Information), although the application of more complex association models was not deemed appropriate. Thus, when analytical ultracentrifugation was used, the component peptides alone behaved as monomers, and, although the experimentally calculated mass for the 1:1:1 mixture was lower than that expected for a fully folded complex, it was consistent with the almost complete folding observed by CD.

(48) O'Shea, E. K.; Klemm, J. D.; Kim, P. S.; Alber, T. *Science* **1991**, *254*, 539−544.
(49) Lumb, K. J.; Kim, P. S. *Biochemistry* **1995**, *34*, 8642−8648.
(50) O'Shea, E. K.; Rutkowski, R.; Kim, P. S. *Science* **1989**, *243*, 538−542.
(51) −100($[\theta]_{222}$ + 3000)/33 000 was used to calculate the percent α-helix: Morrisett, J. D.; Jackson, R. L.; Gotto, A. M., Jr. *Biochim. Biophys. Acta* **1977**, *472*, 93−133.
(52) Jasanoff, A.; Fersht, A. R. *Biochemistry* **1994**, *33*, 2129−2135.

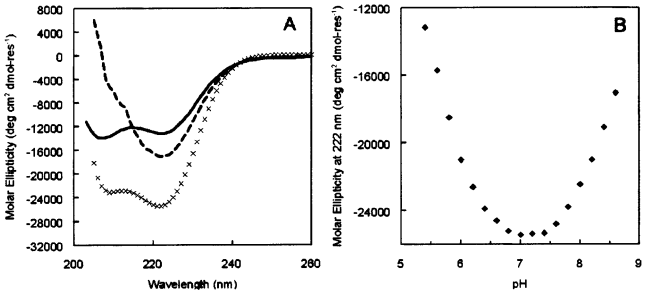

Figure 4. pH stability of the 20 μM belt-and-braces complex. (A) CD spectra for 1:1:1 mixtures of the belt-and-braces peptides recorded at pH 5.4 (solid line), 7 (×), and 8.6 (dashed line). (B) $[\theta]_{222}$ versus pH.

As the belt-and-braces system comprises oppositely charged peptide strands − at neutral pH, the belt is negatively charged and the complementary braces are positive − we probed the α-helical content of the 20 μM 1:1:1 complex in the pH range between 5.4 and 8.6, Figure 4. CD spectra in this range all showed a degree of α-helix, Figure 4A, whereas spectra of the individual peptides as well as the 1:1 mixture of the braces indicated random coil. However, the helical content of the 1:1:1 mixtures fell off rapidly outside the pH range 6.8−7.4, Figure 4B.

Unlike in DNA assembly, where base-pairing specifies partner selection precisely, principles for heterodimeric leucine-zipper association are less clear-cut. As a result, unintended and promiscuous peptide−peptide interactions may occur.[42] To address this issue in the belt-and-braces system, we measured the α-helical content of the two belt-plus-brace binary combinations ($\mathbf{A} + \mathbf{B_N}$ and $\mathbf{A} + \mathbf{B_C}$). Both gave helical CD spectra, but the α-helix content was <60% at 100 μM. Although slightly more helix could be induced with 2:1 brace:belt ratios, the helical content never matched that observed for the 1:1:1 mixtures of the belt-and-braces peptides at similar concentrations, Figure 2B. Furthermore, unlike the sigmoidal thermal unfolding curve observed for the complete ternary mixture, Figure 3, neither of the binary mixtures showed any sign of cooperative unfolding (Figure 1S, Supporting Information). Interestingly, the $\mathbf{A} + \mathbf{B_N}$ combinations were more helical than the $\mathbf{A} + \mathbf{B_C}$ mixtures (data not shown). This fits with the design principles as the $\mathbf{A}$:$\mathbf{B_C}$ interaction was engineered to be less stable, but more specific, than $\mathbf{A}$:$\mathbf{B_N}$ through the inclusion of the asparagine residues at one of the *a* layers of the $\mathbf{A}$:$\mathbf{B_C}$ interface. Thus, we suspect that the $\mathbf{A}$:$\mathbf{B_N}$ interaction is both more stable and more promiscuous than the $\mathbf{A}$:$\mathbf{B_C}$ association; $\mathbf{B_C}$ can only pair with $\mathbf{A}$ at one site (covering heptads 4, 5, and 6), whereas $\mathbf{B_N}$ can potentially pair at two sites (covering heptads 1, 2, and 3 and 2, 3, and 4). As was mentioned above, the first derivative of the thermal unfolding curve for the $\mathbf{A} + \mathbf{B_N}$ mixture provides support for this contention (Figure 1S, Supporting Information).

Assembly of Belt and Braces on Surfaces. The reversible assembly of the belt-and-braces peptides into a complex offers a novel route to decorating solid surfaces with molecular and colloidal components.[11,22−25,53,54] Gold surfaces provide a convenient and potentially useful substrate to test this as the braces each had terminal thiol groups, which are readily chemisorbed onto gold from aqueous solutions. Furthermore, employing gold chips in Biacore allows binding and complex formation to be monitored in real time through surface plasmon resonance (SPR) measurements.[55] For these reasons, we derivatized bare gold Biacore chips with the thiol-containing brace peptides and used the resulting functionalized surfaces to pull down the belt peptide in combination with nonthiol-containing variants of the second brace peptide. To this end, we remade the brace peptides without the terminal cysteine residues, which we refer to as $\mathbf{B_N}$* and $\mathbf{B_C}$*.

Figure 5 shows typical SPR experiments in which the individual braces, and their binary combinations with the belt, were passed over a Biacore sensor chip and the binding was monitored. These were continuous-flow experiments, in which the instrument was first equilibrated with standard running buffer. Peptide-containing solutions were then injected, and, after some defined time, the flow of the running buffer was resumed to wash away any unbound material. As changes in the refractive index of the different buffers and solutions affect the SPR signal, only equilibrium signals − for example, the starting (t_S) and final (t_F) values − can be compared reliably. These signals, quoted in resonance units (RU), were used to gauge the mass of material bound to the surfaces and the percentage of complex formation on the chips.

In general, two types of SPR experiment can be envisaged: either the complex is assembled on a surface by sequential addition of the component peptides, that is, brace, followed by belt, followed by second brace, or one brace is laid down on the surface prior to the addition of a binary mixture of the other brace and the belt. We compared both methods, Figure 5A and B.

For the sequential experiment, a gold chip was treated with $\mathbf{B_C}$, followed by $\mathbf{A}$ and then $\mathbf{B_N}$*, Figure 5A; the surface was washed with running buffer between each peptide addition. The initial binding of $\mathbf{B_C}$ was good, ∼140 RU. Although it has been reported that conformational changes can affect SPR signals,[53] it is generally accepted that the change in RU reflects the mass of material on the surface. As a rule of thumb, 1000 RU corresponds to approximately 1 ng of material.[56] Thus, the 140 RU corresponded to ∼50 fmol of bound brace. However, the subsequent binding of $\mathbf{A}$ (an additional ∼20 RU) and then $\mathbf{B_N}$* (a further ∼10 RU) was poor, Figure 5A; based on the 140 RU of binding for $\mathbf{B_C}$, the maximum theoretical signal for complete $\mathbf{B_C}$:$\mathbf{A}$:$\mathbf{B_N}$* complex formation is $\sim 4 \times 140 = 560$ RU, and we estimated that only ∼7% [((170 − 140)/560 − 140)) × 100] of $\mathbf{B_C}$ was complexed. Presumably, the weak $\mathbf{B_C}$:$\mathbf{A}$ interaction did not sequester enough of $\mathbf{A}$ at the surface (or did not survive the washing step) to allow recruitment of $\mathbf{B_N}$ to complete complex formation. However, the reverse experiment − that is, with $\mathbf{B_N}$ laid down first followed by addition of $\mathbf{A}$ and then $\mathbf{B_C}$* − gave similar results.

In the second approach, Figure 5B, the surface was initially modified with $\mathbf{B_N}$, washed, and then treated with a premixed 1:1 solution of $\mathbf{A}$ and $\mathbf{B_C}$*. After the surface was washed, a steady baseline of ∼230 RU was achieved. This represented an additional 90 RU of binding, which corresponded to ∼21%

(53) Tripet, B.; De Crescenzo, G.; Grothe, S.; O'Connor-McCourt, M.; Hodges, R. S. *J. Mol. Biol.* **2002**, *323*, 345−362.
(54) Lahann, J.; Mitragotri, S.; Tran, T. N.; Kaido, H.; Sundaram, J.; Choi, I. S.; Hoffer, S.; Somorjai, G. A.; Langer, R. *Science* **2003**, *299*, 371−374.
(55) Brockman, J. M.; Nelson, B. P.; Corn, R. M. *Annu. Rev. Phys. Chem.* **2000**, *51*, 41−63.
(56) Finucane, M. D.; Tuna, M.; Lees, J. H.; Woolfson, D. N. *Biochemistry* **1999**, *38*, 11604−11612.

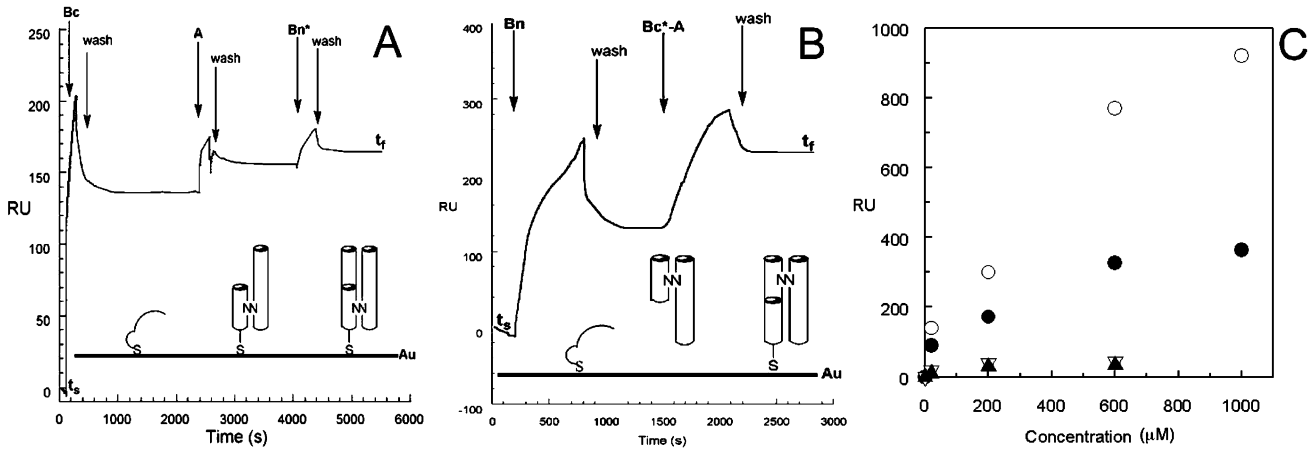

Figure 5. On-surface assembly of belt and braces followed by SPR. (A) Stepwise assembly of a belt-and-braces complex on a sensor chip starting with the coupling of $\mathbf{B_C}$ followed by the addition of **A** and then $\mathbf{B_N}$*. (B) Coupling of $\mathbf{B_N}$ followed by washing and addition of a 1:1 mix of **A** + $\mathbf{B_C}$*. (C) Peptide-concentration dependencies of the coupling of the cysteine-containing braces (○) and subsequent complex formation using the sequential (▲ for **A**, and △ for $\mathbf{B_n}$) and the alternative methods (●). In the schematic representations of the coiled-coil assemblies, N represents asparagines. Conditions: except for the experiments shown in panel D where peptide concentrations were varied, all peptide injections were 50 μL of 20 μM in each peptide in HEPES buffered saline at pH 7.4 and room temperature.

complexation of the sequestered brace. Thus, addition of a binary mix of belt and brace to a surface-bound complementary brace improved complex formation over the sequential assembly method. A similar final intensity (~240 RU) was achieved in the reversed experiment in which the chip was treated with the **A** + $\mathbf{B_C}$ combination followed by $\mathbf{B_N}$*.

These experiments were done using solutions 20 μM in each peptide. At higher concentrations, the binding capacity of the cysteine-containing braces was considerably improved, Figure 5C, for example, >900 RU at 1 mM peptide (i.e., ~320 fmol of brace). Sequential assembly did not improve with increased peptide concentrations. Although the addition of 1:1 belt:brace* mixtures did show increased absolute amounts of complex formation, these appeared to saturate and fall short of 100% complexation of the sequestered brace.

To assess nonspecific peptide binding due to protein adhesion and electrostatic interactions between oppositely charged peptides, two control experiments were carried out: (1) treatment of a $\mathbf{B_C}$-covered chip by similarly charged $\mathbf{B_N}$* showed no binding; (2) a positively charged control coiled-coil peptide − **C**, Ac-CGGYGAQIAALKQQNAALKQQIAALKQ-NH_2 − was engineered as a "false brace" unable to co-assemble with the belt and attach to the surface. As expected, **C** failed to recruit **A** + $\mathbf{B_C}$* mixtures.

The system showed good reversibility: once assembled on the gold surface, the $\mathbf{B_N}$:$\mathbf{B_C}$:**A** complex was readily disassembled and removed by treating with 1 M guanidine hydrochloride. The residual signals were as expected for the binding of the brace peptide(s) alone. These surfaces could either be reused for another round of assembly or be desorbed completely from the surface using mercaptoethanol.[57]

Peptide-Directed Nanoparticle Assembly. If fully folded, the belt-and-braces coiled coil would span 6−7 nm. Thus, the system has potential as a self-assembling nanoscale linker of defined length. We tested this through the assembly of gold nanoparticles to extend the concept of DNA-based nanoparticles assembly, Figure 1A.

The brace peptides, $\mathbf{B_N}$ and $\mathbf{B_C}$, were separately coupled to 15-nm colloidal gold particles to give $\mathbf{B_N}^{Au}$ and $\mathbf{B_C}^{Au}$. After removal of excess, unbound peptide, the derivatized particles were combined. The characteristic red color of the gold suspensions did not change after either peptide coupling or mixing. By UV−vis spectroscopy, the conjugates showed no significant changes in gold-absorbance spectra as compared to unmodified gold particles (data not shown). This is consistent with no assembly taking place and with the design of the belt-and-braces system. In addition, flocculation assays revealed that both of the Au−peptide conjugates were more stable to increased salt (up to 1 M NaCl) than were the bare Au colloids. This behavior is possibly explained in that the brace peptides are positively charged and, so, inhibit particle aggregation and growth. By contrast, addition of the belt peptide to the mixture of brace-peptide-derivatized gold nanoparticles caused a color change and a precipitation of aggregated particles, which settled in the reaction vessel. Moreover, the surface plasmon resonance absorption band associated with the gold nanoparticles for this sample was broadened and red shifted (from 529 to 545 nm) as compared to mixtures lacking the belt peptide, Figure 6. UV−vis spectra for just one type of derivatized gold particle, either $\mathbf{B_N}^{Au}$ or $\mathbf{B_C}^{Au}$, combined with the belt did show a shift, but this was smaller (to 536 nm) and 5 times less intense than that with the complete belt-and-braces system. In summary, these results concur with the CD and SPR data and indicate that although there were some promiscuous belt−brace interactions the complete **A** + $\mathbf{B_N}$ + $\mathbf{B_C}$ system produced the most competent and stable assemblies.

Nanoparticle assemblies were visualized directly by transmission electron microscopy (TEM), Figure 7. As was seen by others working with colloidal precipitates,[15] we observed both 3-D and 2-D networks, Figure 7A, B, and C, respectively. The former could not be analyzed with any certainty, but the 2-D networks showed uniformly separated particles at distances of 7.22 ± 0.34 nm. These measurements are consistent with a folded six-heptad coiled-coil linker. The networks were found exclusively in preparations containing all three belt-and-braces components, $\mathbf{B_N}^{Au}$, $\mathbf{B_C}^{Au}$, and peptide **A**: under similar condi-

(57) Demers, L. M.; Mirkin, C. A.; Mucic, R. C.; Reynolds, R. A., III; Letsinger, R. L.; Elghanian, R.; Viswanadham, G. *Anal. Chem.* **2000**, *72*, 5535−5541.

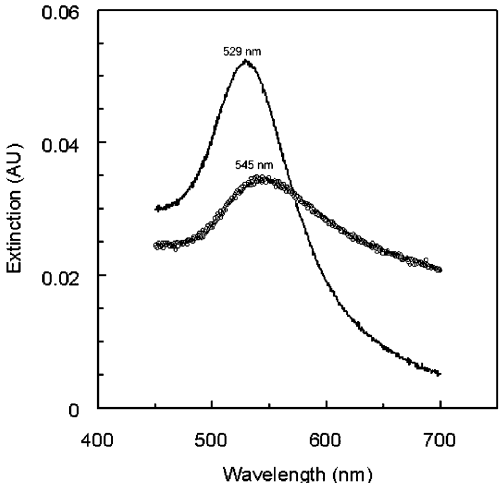

Figure 6. UV−visible spectra for the 1:1 $\mathbf{B_N}^{Au}$:$\mathbf{B_C}^{Au}$ mixture before (solid line) and after (○) adding a stoichiometric amount of peptide **A**, the belt.

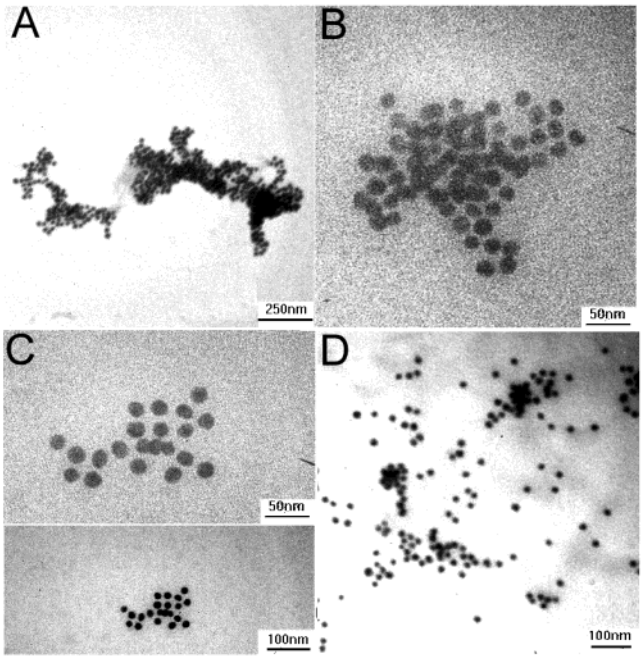

Figure 7. Direct observation of peptide-mediated nanoparticle assembly. TEM images of ordered three-dimensional (A, B) and two-dimensional (C) gold-nanoparticle networks formed by mixing $\mathbf{B_N}^{Au}$, $\mathbf{B_C}^{Au}$, and peptide **A** in a 1:1:1 ratio. (D) A typical collidal material from a mixture of the linker with one brace ($\mathbf{B_N}^{Au}$ or $\mathbf{B_C}^{Au}$) in 1:1 or 1:2 ratios.

tions, bare gold colloids displayed only closely aggregated particles without distinct spacings indicative of nonspecific particle-growth processes. Similarly, in the mixtures of peptide **A** with $\mathbf{B_N}^{Au}$ or $\mathbf{B_C}^{Au}$, single particles and nonuniform aggreagtes dominated, Figure 7D.

Further CD experiments tested whether the belt-and-braces peptides were fully folded in the presence of the gold nanoparticles, Figure 8: in the absence of the belt peptide, a mixture of $\mathbf{B_N}^{Au}$ and $\mathbf{B_C}^{Au}$ gave a random-coil signal as expected; a mixture of $\mathbf{B_N}^{Au}$ + **A** was ~50% helical, whereas mixtures with all three peptide components were ~70% helical or more. Interestingly, the $\mathbf{B_N}^{Au}$ + $\mathbf{B_C}^{Au}$ + **A** mixture was ~10% less helical than the $\mathbf{B_N}$ + $\mathbf{B_C}^{Au}$ + **A** sample. It is unlikely that this loss in helix is due to unwinding of the belt-and-braces coiled coil; more likely, the bulky nanoparticles reduce complex

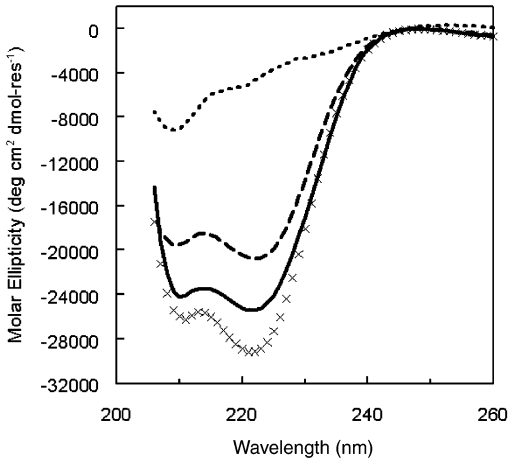

Figure 8. Folding of the nanoparticle-bound peptides. CD spectra for the following equimolar mixtures: $\mathbf{B_N}^{Au}$ + $\mathbf{B_C}^{Au}$ (dotted line); $\mathbf{B_N}^{Au}$ + **A** (dashed line); $\mathbf{B_N}^{Au}$ + $\mathbf{B_C}^{Au}$ + **A** (solid line); $\mathbf{B_N}^{Au}$ + $\mathbf{B_C}^{Au}$ + **A** (×).

formation to a certain extent or this effect is due to light-scattering commonly observed for particulate systems.

Summary

To summarize, we describe a novel, self-assembling, nanoscale, peptide-based linker. The system comprises three leucine-zipper peptides of de novo design: the longer peptide, **A** or "the belt", acts as a template for the co-assembly of two half-sized peptides, $\mathbf{B_N}$ and $\mathbf{B_C}$, also termed "the braces". The basic features of the design were confirmed in solution by CD spectroscopy and analytical ultracentrifugation, which indicated a predominantly α-helical, ternary assembly. These assemblies were thermally stable and unfolded reversibly. Although specific positive and negative features were included in the design, some promiscuous belt−brace interactions were observed. However, these were not cooperatively folded structures and were thermally labile. Using SPR experiments in Biacore, we demonstrated the assembly of the complex on gold surfaces. This was best effected by first coupling one of the brace peptides to the surface via a thiol group, followed by co-assembly with a binary mixture of the belt and the other brace, that is, rather than by sequentially adding the component peptides to the surface. The utility of the system in bringing together peptide-bound cargo was demonstrated using colloidal gold nanoparticles. The braces were used to derivatize the particles, which were then brought together to form nanoscale networks by adding the belt. TEM images of these networks revealed that the particles were regularly separated by ~7 nm, fully consistent with the six-heptad design of the belt-and-braces coiled coil. In accord with this, CD experiments confirmed that the majority of the peptide linkers were folded when bound to gold nanoparticles.

To our knowledge, belt-and-braces is a novel concept in coiled-coil assembly and the first example of employing rationally designed peptides to guide nanoparticle assembly, which, hitherto, has been achieved using DNA-based linkers of some description.[8,12−25] Although the field of DNA-directed assembly is more mature at present, peptides potentially offer some advantages over DNA in such applications. Specifically, synthetic genes for peptide sequences can be synthesized and cloned for use in recombinant DNA technologies. In this case, for protein cargos, the braces need not be added chemically,

but brace-protein fusions could be engineered recombinantly. This possibility may unlock exciting new routes to enable the generation of novel and functional protein-based supramolecular and nanostructured assemblies and biosensors.[58]

Experimental Section

Materials and Methods. A Pioneer Peptide Synthesis System (PE Applied Biosystems, CA) was used for peptide assembly. All reagents and resins were purchased from Applied Biosystems (Warrington, UK) or CN Biosciences (Nottingham, UK). Colloidal gold nanoparticles (15 nm) were obtained from ICN Biomedicals Gmbh (Eschwege, Germany). Analytical and semipreparative gradient RP-HPLC was performed on a JASCO HPLC system (model PU-980, Tokyo, Japan) using Vydac C_{18} analytical (5 μm, 4.6 mm i.d. $\times$ 250 mm) and semipreparative (5 μm, 10 mm i.d. $\times$ 250 mm) columns. Both analytical and semipreparative runs used a 20−40% B gradient over 45 min at 4.7 mL/min (semipreparative) and 1 mL/min (analytical) where buffer A was 5% aqueous CH_3CN, 0.1% TFA, and buffer B was 95% aqueous CH_3CN, 0.085% TFA. Mass spectra were recorded on a TofSpec E Matrix Assisted Laser Desorption Ionization (MALDI) spectrometer (Micromass Ltd, Manchester, UK). Analytical ultracentrifugation was performed using a Beckman Optima XL-I analytical ultracentrifuge fitted with an An-60 Ti rotor. CD experiments were conducted on a JASCO J-715 spectropolarimeter fitted with a Peltier temperature controller (Tokyo, Japan). SPR experiments were carried out on a BIACORE 2000 instrument (Biacore AB, Uppsala, Sweden). TEM data were acquired using a Hitachi 7100 transmission electron microscope (Tokyo, Japan), fitted with a charge-coupled device camera from Digital Pixel Co. Ltd. (Brighton, UK) and software from Kinetic Imaging Ltd. (Liverpool, UK).

Peptide Synthesis. Peptide synthesis was carried out by the combination of standard Fmoc/^{t}Bu solid-phase protocols with TBTU/DIPEA as coupling reagents on a PEG-PS-resin for carboxyl-free peptides and using a PAL linker for peptide amides. A 95% TFA mixture (95:2.5:2.5 TFA/water/TIS) was used as the postsynthesis cleavage cocktail for noncysteine peptides. For the deprotection of the cysteine-containing peptides, another 93.5% TFA mixture (93.5:2.5:2.5:1.5 TFA/water/EDT/TIS) was used. The purification of all peptides used semipreparative RP-HPLC, and the purities were confirmed by analytical RP-HPLC.

Mass Spectrometry. Peptide identities were verified by MALDI-Tof mass spectrometry with α-cyano-4-hydroxycinnamic acid as the matrix: peptide **A** $[M + H]^+$ *m/z* 4624.2 (calc), 4625.4 (found), $[M + 2H]^{2+}$ *m/z* 2313 (found); peptide $\mathbf{B_N}$ $[M + H]^+$ *m/z* 2570 (calc), 2571.2 (found), $[M + K]^+$ *m/z* 2609.7 (found); peptide $\mathbf{B_N}$* $[M + H]^+$ *m/z* 2354 (calc), 2354.8 (found); peptide $\mathbf{B_C}$ $[M + H]^+$ *m/z* 2528.1 (calc), 2529.3 (found), $[M + Na]^+$ *m/z* 2551.1 (found), $[M + K]^+$ *m/z* 2567.2 (found); peptide $\mathbf{B_C}$* $[M + H]^+$ *m/z* 2311.9 (calc), 2312.3 (found), $[M + Na]^+$ *m/z* 2334.8 (found); peptide **C** $[M + H]^+$ *m/z* 2826.3 (calc), 2828.3 (found), $[M + 2H]^{2+}$ *m/z* 1413.2 (found), $[M + K]^+$ *m/z* 2865.4 (found).

Sedimentation Equilibrium Experiments. These experiments were conducted at 5 °C. 100 μL samples of 100 μM peptide **A** or mixtures of the braces, and the linker plus both braces, with initial A_{280} values being 0.15, 0.147, and 0.144, respectively, in the 1.2 cm path length cells used, were buffered to pH 7 with 10 mM MOPS containing 1 mM DTT and 100 mM sodium chloride. Samples were equilibrated for 48 h at 30 000, 37 500, and 55 000 rpm. Sedimentation equilibrium curves were measured by the absorbance at 280 nm. The resulting data were fitted simultaneously using routines in the Beckman Optima XL-A/XL-I data analysis software (version 4.0). The density of the buffer at 5°C was taken as 1.005 mg/mL. Based on the amino acid composition, the averaged partial specific volume for the peptides was calculated to be 0.75 mL/mg for peptide **A**, 0.774 mL/mg for $\mathbf{B_N}$/$\mathbf{B_C}$, and 0.77 mL/mg for the equimolar mixture of **A**, $\mathbf{B_N}$, and $\mathbf{B_C}$.

Circular Dichroism Spectroscopy. All data for peptide samples prepared in 10 mM MOPS (pH 7) were collected in 1-mm quartz cuvettes. Data points for CD spectra were recorded at 1-nm intervals using a 1-nm bandwidth and 4−16-s response times. After baseline correction, ellipticities in mdeg were converted to molar ellipticities (deg cm^2 dmol res^{-1}) by normalizing for the concentration of peptide bonds. Data points for the thermal unfolding curves were recorded through 1 °C/min ramps using a 2-nm bandwidth, averaging the signal for 8 s at 1 °C intervals. Data for pH experiments were obtained for peptide samples in 10 mM EPPS (basic pH) and MES (acidic pH) buffers.

Surface Plasmon Resonance (SPR). SPR sensograms were recorded at 20 °C on a BIACORE 2000 instrument using standard procedures and buffers (HBS running buffer (10 mM HEPES, 0.15 M NaCl, 0.005% Surfactant P20, 50 μM EDTA (pH 7.4))). Peptide solutions were 20 μM unless otherwise stated. Bare gold sensor chips were used throughout the studies. These allowed a simple and reversible strategy for assembling thiol-containing braces followed by a belt-plus-brace mixture on solid surfaces.

Preparation of Peptide−Nanoparticle Conjugates. Gold nanoparticle conjugates were synthesized by treating 15 nm gold nanoparticles (1 mL of a 1 nM aqueous solution) separately with peptides $\mathbf{B_C}$ and $\mathbf{B_N}$ (25 μL of 3 mM solutions, to give final peptide concentrations of 73 μM). After standing overnight, the solution was centrifuged at 14 000 rpm. The supernatant was removed, and the red sediment was washed twice and resuspended in water. ~65−80% of the original Au nanoparticle concentration was recovered.

UV−Visible Spectroscopy. UV/vis spectra were recorded on a Hitachi U3000 spectrometer. Quantification of the Au−peptide conjugates and spectral measurements of the aggregation experiments were carried out at room temperature in water.

Transmission Electron Microscopy. Unless stated otherwise, samples of Au−peptide conjugates were mixed 1:1 with peptide **A** (20−100 μM) in filtered MOPS buffer (10 mM, pH 7) and incubated at 20 °C for 30−60 min. Aliquots of the mixtures were applied to carbon-coated copper specimen grids (Agar Scientific Ltd, Stansted, UK) and dried with filter paper at room temperature. Grids were examined by a TEM at 100 kV, and digital images (800 $\times$ 1200 pixel) were recorded for analysis. Separations between neighboring particles were measured and averaged over 300 pairs; the standard deviation of these measurements was 0.34 nm (Figure 3S, Supporting Information). The sizes of the nanoparticles (15 nm) were confirmed with a standard deviation of 1 nm.

Acknowledgment. We thank the members of the D.N.W. and C.M.N. groups for advice and the BBSRC of the UK for financial support (grant E13753). C.M.N. and B.C. acknowledge financial support from Deutsche Forschungsgemeinschaft, DFG, SPP 1072.

Supporting Information Available: A list of abbreviations together with figures of additional data for certain thermal denaturation, analytical ultracentrifugation, and electron microscopy experiments mentioned in the text (PDF). This material is available free of charge via the Internet at http://pubs.acs.org.

JA0352045

(58) Niemeyer, C. M. *Trends Biotechnol.* **2002**, *20*, 395−401.